Received: 25 July 2016 | Accepted: 5 January 2017

DOI: 10.1111/jace.14780

ORIGINAL ARTICLE

Journal of the American Ceramic Society

Grain growth and pore coarsening in dense nano-crystalline UO_{2+x} fuel pellets

Tiankai Yao[1] | Kun Mo[2] | Di Yun[2,3] | Sonal Nanda[1] | Abedellatif M. Yacout[2] | Jie Lian[1]

[1]Department of Mechanical, Aerospace, and Nuclear Engineering, Rensselaer Polytechnic Institute, Troy, New York

[2]Nuclear Engineering Division, Argonne National Laboratory, Lemont, Illinois

[3]School of Nuclear Science and Technology, Xi'an Jiaotong University, Xi'an, Shaanxi, China

Correspondence
Jie Lian, Department of Mechanical, Aerospace, and Nuclear Engineering, Rensselaer Polytechnic Institute, Troy, NY
Email: lianj@rpi.edu

Funding information
U.S. Department of Energy under Contract between UChicago Argonne, LLC and the Department of Energy., Grant/Award Number: No. DE-AC-02-06CH11357; U.S. NSF career, Grant/Award Number: 1151028; US DOE Nuclear Energy University Program (NEUP), Grant/Award Number: DE-NE0008440; US DOE Nuclear Energy Advanced Modeling and Simulation (NEAMS) program

Abstract

Dense nano-sized UO_{2+x} pellets are synthesized by spark plasma sintering with controlled stoichiometries ($UO_{2.03}$ and $UO_{2.11}$) and grain sizes (~100 nm), and subsequently isothermally annealed to study their effects on grain growth kinetics and microstructure stability. The grain growth kinetics is determined and analyzed focusing on the interaction between grain boundary migration, pore growth, and coalescence. Grains grow much bigger in nano-sized $UO_{2.11}$ than $UO_{2.03}$ upon thermal annealing, consistent with the fact that hyper-stoichiometric UO_{2+x} is beneficial for sintering due to enhanced U ion diffusion from excessive O ion interstitials. The activation energies of the grain growth for $UO_{2.03}$ and $UO_{2.11}$ are determined as ~1.0 and ~2.0 eV, respectively. As compared with the micrometer-sized UO_2 in which volumetric diffusion dominates the grain coarsening with an activation energy of ~3.0 eV, the enhanced grain growth kinetics in nano-sized UO_{2+x} suggests that grain boundary diffusion controls grain growth. The higher activation energy of more hyper-stoichiometric nano-sized $UO_{2.11}$ may be attributed to the excessive O interstitials pinning grain boundary migration.

KEYWORDS
grain growth, pore, stoichiometry, UO_2

1 | INTRODUCTION

Oxide fuels with an initial microstructure of 5 vol. % porosity and grain size of ~10 μm experience a drastic microstructure evolution upon burning in reactor environment such as densification, grain coarsening into columnar structure, and center void formation. At high burnup with extensive fission reaction, e.g., above ~50 GWd/tHM, depending on degree of enrichment and neutron flux spectrum,[1] a high burnup structure (HBS) forms at the rim regime of the fuel pellets. Original ~10 μm grains transfer to nanocrystalline (hereafter referred as nc-) microstructure with an average grain size of 100-300 nm due to grain subdivision. HBS is an essentially hierarchical mesoporous structure in which micrometer-sized intergranular pores are embedded in a dense nc-UO_2 matrix. As compared with original UO_2 fuel pellets, the HBS is considered as an advanced fuel form with enhanced thermal conductivity and radiation resistance due to the essential nature of nanostructure materials, and greater fission gas retention capability.[2] The formation mechanism of HBS is not yet well understood,[1] and it is generally believed to be a competition between radiation-induced grain subdivision and radiation/thermally-induced grain coarsening. The unique size and distribution of pores in HBS further complicate the stability of HBS at thermal and irradiation conditions, coupled with the complexity of fuel chemistry evolution into a more hyper-stoichiometric composition upon uranium burning.[3] The microstructure evolution and grain coarsening have profound impacts on fuel properties such as thermal-mechanical properties, fuel swelling, and fission gas retention capability.

Grain growth kinetics of bulk 10-20 μm sintered standard UO_2 fuels (hereafter referred as bulk-UO_2) has been extensively studied to correlate UO_2 grain size with fuel burnup so as to estimate fuel performance and working temperature.[4,5] However, few studies on the microstructure evolution of the nc-UO_2 matrix as identified in HBS structure are available, limiting the understanding of the stability mechanisms of HBS and its consequent impacts on fuel performance. The microstructure evolution and fuel properties evaluation are critical for developing high-fidelity multi-physics MARMOT models[6] in predicting fuel performance under the DOE Nuclear Energy Advanced Modeling and Simulation program. However, challenges exist in investigating microstructure evolution and its impact on fuel properties of the nc-UO_2 matrix as multiple microstructure features including grain size, pore distribution, and fuel chemistry affects are coupled together affecting fuel properties. It is necessary to synthesize clean UO_2 materials with controlled microstructures such that the impact of the microstructure features can be probed separately.

In this paper, dense nc-UO_{2+x} pellets (>95% theoretical density, TD) with controlled stoichiometries and grain sizes were fabricated by a high-pressure spark plasma sintering (SPS) process, serving as the model systems for investigating grain growth kinetics of the nc- UO_2. The SPS-fabricated nc-UO_{2+x} pellets were thermally annealed under an argon atmosphere, and the grain growth kinetics was determined focusing on the effects of the stoichiometry and grain size. The activation energy of grain growth for the nc-UO_{2+x} with different stoichiometries was also determined and compared with literature data based on bulk UO_2 and molecular dynamics (MD) simulations. Grain boundary diffusion is suggested to be the dominant mechanism for the greatly enhanced grain growth kinetics for the nc-UO_{2+x} pellets.

2 | EXPERIMENTAL DETAILS

Bulk dense nc-UO_{2+x} pellets with various length scales were sintered and densified by SPS (Thermal tech® SPS10-3, Santa Rosa, CA), a field-assisted sintering technology (FAST), from nano-sized UO_{2+x} powders with two different stoichiometries (2.03 and 2.11) prepared by high energy ball milling (Fritsch, Pulverisette 7, Idar-Oberst, Germany). Sintering of the dense UO_{2+x} pellets were conducted in argon atmosphere using high-pressure WC dies assembling (for a detailed description, please see Ref. [7]). After sintering, the density of the pellets was measured according to Archimedes' principle at room temperature using distilled water as the immersion media. Relative density is calculated with respect to 10.97 g/cc for theoretical density of UO_2.

The lattice parameter, a, was calculated from X-ray diffraction (XRD) peak positions, collected using Copper Ka (wavelength: 0.15418 nm) at a scanning step size of 0.013 (PANalytical Inc., Westborough, MA). The stoichiometry of both powder and bulk pellets was calculated from the UO_2 lattice parameter based on the following equation[8]: a=5.4705−0.132x, where a is the lattice parameter for UO_{2+x} in Å; and x is the deviation of stoichiometry from a perfect O/U ratio of 2. Physical properties of the sintered UO_{2+x} pellets are listed in Table 1. Based on estimated stoichiometry, no significant reduction and stoichiometric change occurred during sintering process due to usage of the WC dies[9] and assembly instead of graphite dies. The detailed correlation of the sintering processing-microstructure control-physical properties of the sintered nc-UO_{2+x} was also determined and reported separately.

Isothermal annealing of the sintered nc-UO_{2+x} pellets was conducted in a MTI® GSL-1100X-UL (MTI Corp. St, Richmond, CA) tube furnace under a neutral atmosphere of Ar gas (150 mL/min) at temperatures ranging between 700°C and 900°C from 0.5 to 8 hours. After annealing, the tube furnace was quenched down to room temperature by forced blowing of compressed air along the quartz tube to effectively preserve grain structure. Scanning electron microscopy imaging was performed on fractured surfaces and quantitatively analyzed manually using Image J[10] over 200 grains to measure the morphology and evaluate grain structure, specifically grain size and pore distribution.

Grain growth data obtained as functions of annealing temperatures and durations were fitted by grain growth kinetics using MATLAB with 95% confidence bounds based on the following equation:

$$D^n - D_0^n = k_0 e^{\left(\frac{-Q}{RT}\right)} t^m, \quad (1)$$

where D is the grain size of the sintered UO_{2+x} pellets after annealing at a certain temperature for a given span of time, D_0 is the starting grain size of the sintered UO_{2+x} pellets, n is the grain growth exponent, k_0 is a fitting constant, Q is the grain growth activation energy, R is the gas constant, T is the annealing temperature in K, t is the annealing time in hour, and m is the time exponent. Fitted n value based on Equation (1) for each condition is subsequently used to drive time exponent m and activation energy Q.

TABLE 1 Summary of physical properties of the sintered nano UO_2 pellets

Sample	Porosity /%	Grain size/nm	Stoichiometry
$UO_{2.03}$-103 nm	4.0 ± 1.1	103 ± 3	2.03 ± 0.02
$UO_{2.03}$-144 nm	1.3 ± 0.7	144 ± 6	2.03 ± 0.02
$UO_{2.11}$-63 nm	3.8 ± 1.0	63 ± 3	2.11 ± 0.03
$UO_{2.11}$-165 nm	1.6 ± 0.4	165 ± 5	2.11 ± 0.03

Conducting natural log on both sides of Equation (1) leads to following equation:

$$\ln\left(D^n - D_0^n\right) = \ln K_0 - \frac{Q}{R} \times \frac{1}{T} + m \ln t$$

As a result, plot of $\ln\left(D^n - D_0^n\right)$ with respect to $\frac{1}{T}$ provides the value of $\left(-\frac{Q}{R}\right)$, which is the slope of the plot that yields the activation energy of grain growth (Q). Similarly, plot of $\ln\left(D^n - D_0^n\right)$ with respect to $\ln t$ delivers the value of m.

3 | RESULTS AND DISCUSSION

U ion exhibits three distinct valence states: 4+, 5+, and 6+, and UO_2 can be easily oxidized to hyperstochiometric compositions with O/U ratios beyond 2. Depending on the oxidizing conditions, UO_2 fluorite crystal structure can accommodate various amounts of oxygen interstitials and transform into transient phases, such as U_4O_9 and U_3O_7, prior to the thermodynamically stable U_3O_8 phase.[11] Before transforming to U_4O_9, the solid solution of O interstitials with UO_2 is denoted as UO_{2+x}. Depending on the local configuration, the O interstitials of UO_{2+x} exists in various configurations, including mono-interstitial, di-interstitials, split di-interstitials, and Willis defect.[12]

Excessive O interstitials generate surplus U vacancies according to the Schottky defect equilibrium principle.[13] The proliferation of U vacancies significantly enhances volumetric diffusion of U ions to promote powder sinterability[14] and grain growth.[15] A previous study[16] showed that an oxidizing environment can significantly lower the grain growth activation energy of bulk UO_2 from ~80 to 50 cal/mol. Given the substantial effect of excessive O interstitials on grain growth of UO_2, it is of great necessity to maintain the stoichiometry of the nc-UO_{2+x} during grain growth study.

Ar gas is widely used as a neutral environment to study grain growth of both stoichiometric UO_2[16] and hyper-stoichiometric UO_{2+x}.[17] High-temperature (1400°C) annealing in Ar atmosphere was applied to anneal out the irradiation effects caused by alpha decay from plutonium in MOX fuel.[18] In this study, XRD spectra obtained from the nc-$UO_{2.03}$ pellets before and after 4 hours annealing at 900°C in Ar gas environment showed neither detectable peak shifting nor shoulder peaks at higher angles for U_4O_9 (Figure 1). These results indicate that the stoichiometry was well preserved during the isothermal annealing process. Therefore, the impact of possible stoichiometry change upon isothermal annealing on grain growth kinetics can be avoided.

Figure 2 shows the typical microstructural evolution of $UO_{2.03}$-103 nm pellets after different durations of annealing at 700°C. Grains grow from the initial size of 103 nm to 155, 166, 189, 239, and 238 nm after 0.5, 1, 2, 4, and 8 hours of annealing, respectively. Pores also grow from ~20 nm to ~80 nm and migrate with grain boundaries. The surfaces of individual grains are smooth and clean, and remain unchanged throughout the annealing process, indicating that the stoichiometry of these pellets is close to stoichiometric 2.0,[19] consistent with the XRD results (Figure 1). Further increase of the annealing temperature to 800°C and 900°C leads to grain growth and pore coarsening with similar characteristics but to larger sizes proportional to annealing temperatures.

Grain coarsening was also observed in the hyper-stoichiometric nc-$UO_{2.11}$ pellets with a continuous grain size increase upon isothermal annealing (Figure 3). As compared with the nc-$UO_{2.03}$, two distinct features were observed: (i) significantly larger grains (for example, grain size reaches ~500 nm at 700°C in 8 hours); and (ii) pore coalescence into interconnected micrometer-sized pores. Compared with $UO_{2.03}$ in which pores evenly distributed along grain boundaries, the pores in the $UO_{2.11}$-63 nm pellet grew and coalesced even after 1 hour of annealing at 700°C. Shallow stepped-patterns on grain surfaces, as evidenced on Figure 3F, suggest a stoichiometry close to ~2.15.[19] This is also consistent with the stoichiometry of 2.11 estimated by XRD measurement.

Figure 4 summarizes the microstructural evolution of the dense nc-UO_{2+x} pellets after 8 hrs annealing at different temperatures. Combined with Figure 5 which shows grain size evolution, the following observations can be made:

1. Grain size increases exponentially with time in a relatively short time less than 2 hours upon isothermal

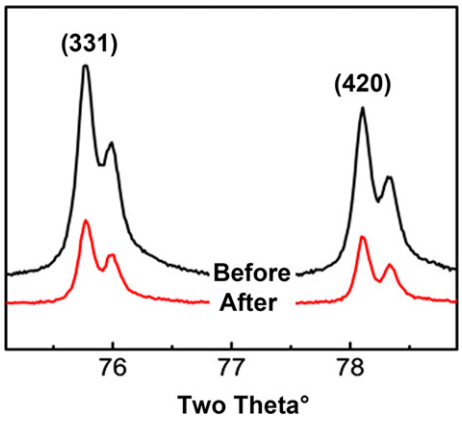

FIGURE 1 XRD spectra of the $UO_{2.03}$-103 nm pellet before and after annealing in a tube furnace at 900°C for 4 h. No peak shift is observed, suggesting unchanged stoichiometry upon isothermal annealing in Ar environment [Color figure can be viewed at wileyonlinelibrary.com]

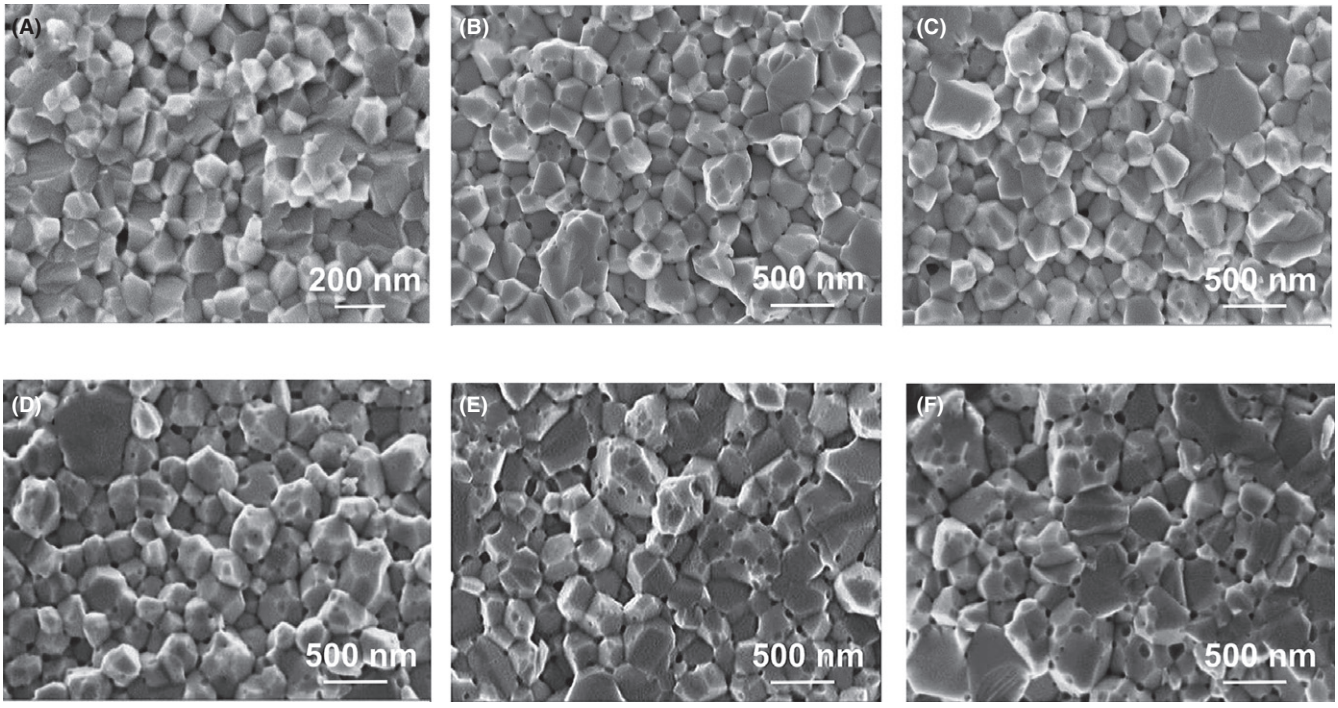

FIGURE 2 Grain growth and pore coalescence in the $UO_{2.03}$-103 nm pellet at 700°C for (A) as sintered, (B) 0.5 h, (C) 1 h, (D) 2 h, (E) 4 h, and (F) 8 h isothermal annealing

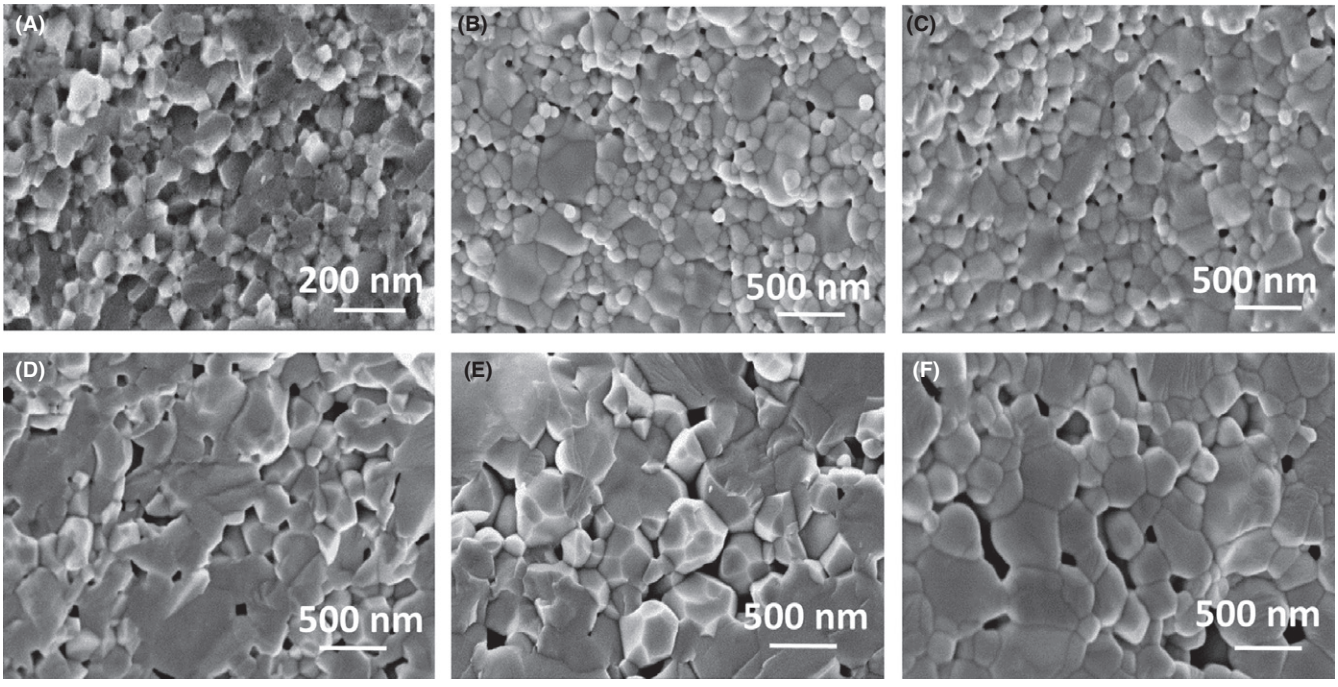

FIGURE 3 Grain growth and pore coalescence in the $UO_{2.11}$-66 nm pellet at 700°C (A) as sintered, (B) 0.5 h, (C) 1 h, (D) 2 h, (E) 4 h, and (F) 8 h isothermal annealing

annealing, and then saturates due to the loss of driving force resulting from curvature driven-growth process;

2. Higher annealing temperatures leads to larger grains as a result of enhanced grain boundary mobility;
3. A dramatic morphological difference and pore growth behavior are observed in the two hyper-stoichiometric UO_{2+x} samples. Closed inter-granular pores are prevalent in $UO_{2.03}$ pellets while pores in $UO_{2.11}$ pellets

grow to significantly larger sizes and coalesce upon annealing;

4. Few intra-granular pores are observed in all pellets, indicating pore grows and migrates with grain boundaries regardless of grain sizes, stoichiometries, and porosity;
5. Starting at similar grain sizes, grain growth in $UO_{2.11}$ pellets is more substantial than $UO_{2.03}$ pellets as evidenced by much bigger grain sizes after thermal annealing.

The isothermal annealing-induced grain coarsening to larger sizes for nc-$UO_{2.11}$ than $UO_{2.03}$ is consistent with the fact that hyper-stoichiometric UO_{2+x} is typically used for fuel sintering and fabrication. Excessive O ions in hyper-stoichiometric UO_{2+x} occupy interstitial positions, leading to surplus U ion vacancies and enhancing the U ion diffusion rate and thus powder densification.

The grain growth exponent (n) (Figure 5) of the nc-$UO_{2.11}$ pellets is determined to be ~2.0. For near-stoichiometric nano-sized $UO_{2.03}$ pellets, the grain growth exponent is derived as ~2.5. This grain growth exponent was also identified for bulk UO_2 under various environments, such as Ar, vaccum, H_2, and CO_2.[20] MD simulation showed that the grain growth of dense CeO_2 with a low porosity ~1% also yielded a grain growth exponent of 2.5.[21] Classical curvature-driven grain growth has a growth exponent of 2, but is found to be only applicable for high-purity metals where there is no dragging force on grain boundary movement from either secondary solutes or pores. Derived time exponents (Figure 6) show overall good linear fitting features. For pure curvature-driven grain growth, the time exponent should have a unit value; however, the derived time exponent for this study is smaller than 1.

It is noteworthy that the derived low activation energies (1-2 eV) (Figure 7) for grain growth of the dense nc-UO_{2+x} pellets are significantly smaller than the previously reported values for bulk UO_2[22] and from MD simulations (3.06 eV) in which a bi-crystal model was applied.[23] Converted values of activation energies in other units (inserted

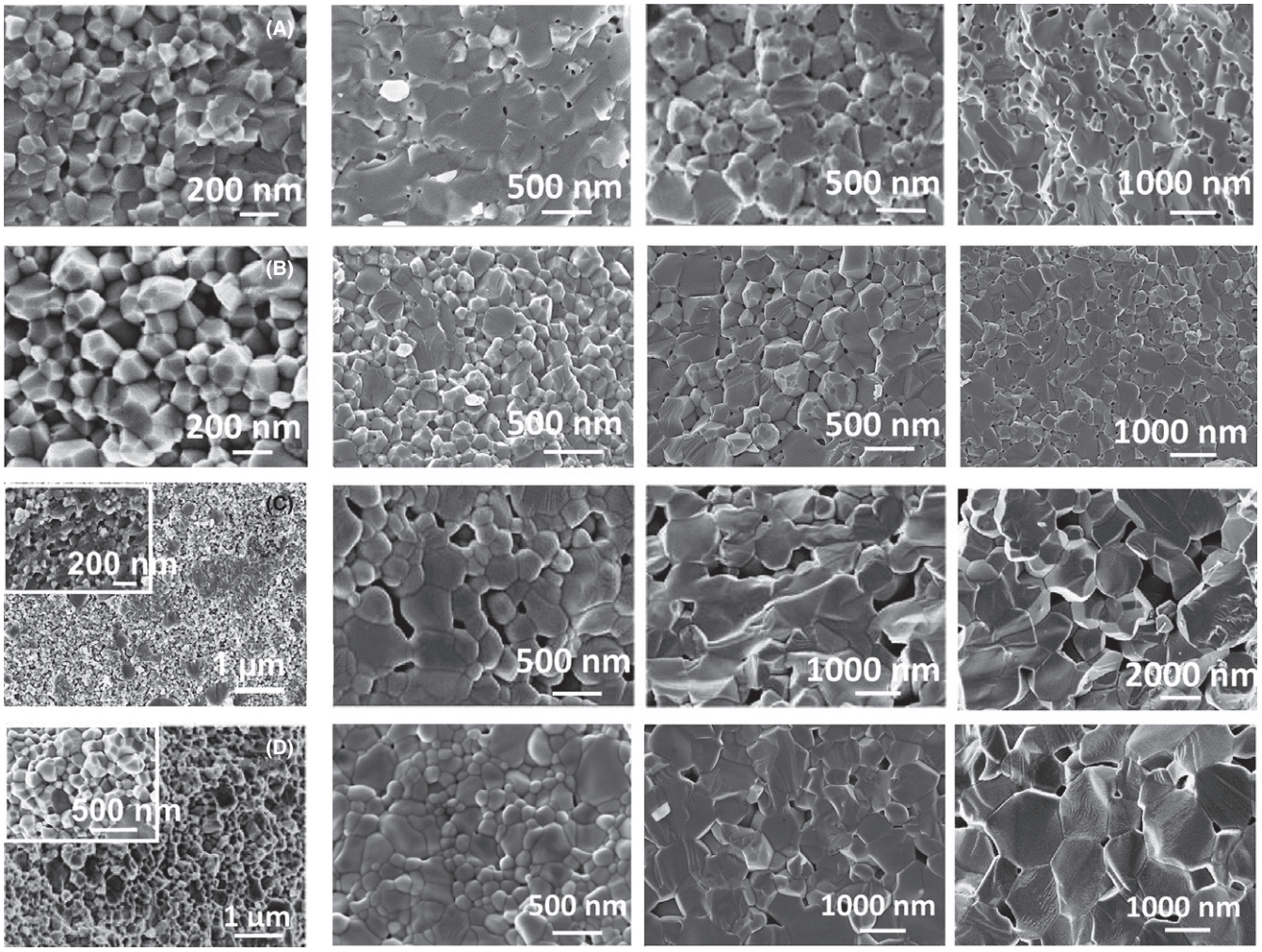

FIGURE 4 Microstructure features of the $UO_{2.03}$-103 nm (A), $UO_{2.03}$-144 nm (B), $UO_{2.11}$-66 nm (C), and $UO_{2.11}$-165 nm (D) in as-sintered condition (first column), after annealing at 700°C (second column), 800°C (third column), and 900°C (fourth column) all for 8 h

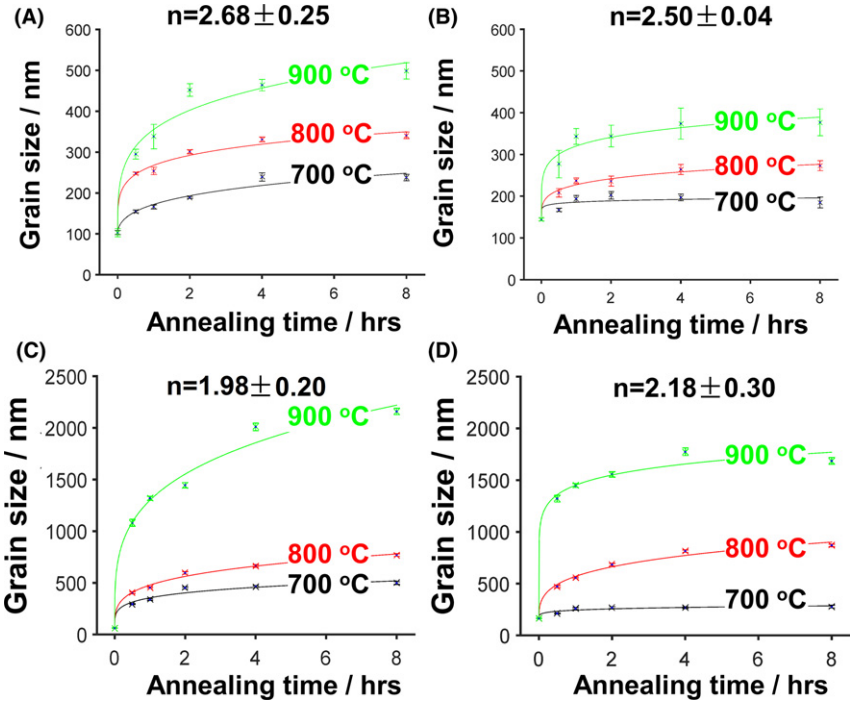

FIGURE 5 Grain coarsening and growth components for (A) the $UO_{2.03}$-103 nm, (B) $UO_{2.03}$-144 nm, (C) $UO_{2.11}$-66 nm, and (D) $UO_{2.11}$-165 nm pellets [Color figure can be viewed at wileyonlinelibrary.com]

in Figure 7) indicate that the energies are much smaller than literature reported values for U ion volumetric diffusion (70-108 Kcal/mol).[17,25–27] This suggests that other than volumetric diffusion, other mass transport mechanisms, such as grain boundary diffusion, may dominate mass transport for the low temperature grain growth behavior of the dense nc-UO_{2+x} pellets.

Particularly, grain boundaries could drastically facilitate mass transportation and increase atoms diffusion at grain boundaries and near grain boundary regions. By measuring diffusion of ^{237}U tracer in bulk-UO_2 at temperature range of 1900°C-2150°C, a significant contribution of grain boundary diffusion was revealed whereas contribution of volumetric diffusion is negligible.[25] The grain boundary diffusion rate of U ions, with a supposed boundary thickness of 5 Å, was generally found to be 10^5 times higher than the volumetric diffusion rate. Very recently, U ion self-diffusion coefficient near grain boundaries was also found to be five orders magnitude higher than volumetric diffusion in single crystals between 1498°C and 1697°C.[27] A simulation study also reported the migration energy for U ions near grain boundary regions is as low as 0.8 eV, and the energy even lowers to 0.5 eV at grain boundaries.[28] On the contrary, the simulated values for vacancy migration and interstitial migration for volumetric diffusion are 4.4 and 5.8 eV,[29] respectively, much higher than grain boundary diffusion energies of U ions. The activation energy (~1.0 eV) of grain growth derived for the near-stoichiometric nc-$UO_{2.03}$ pellets is significantly lower than the ones required for volumetric diffusion of U ions. The derived activation energies are consistent with the simulation results found for the enhanced migration energy for U ions near or at grain boundary,[28] indicating grain boundary diffusion is the dominant mass transport mechanism for the grain growth of the dense nc-$UO_{2.03}$ pellet.

Hyper-stoichiometric nano-sized $UO_{2.11}$ displays greater activation energies for grain growth as compared to more stoichiometric $UO_{2.03}$, which may be attributed to the interaction between O interstitials and grain boundaries. The excess O interstitials in hyper-stoichiometric UO_{2+x} introduce extra U vacancies in the U sublattice to promote the U diffusion through the vacancy mechanism, beneficial for the fuel sintering and densification. However, the excessive oxygen interstitials can also pin grain boundaries and impedes grain boundary movement, resulting in increased activation energies for grain growth. A similar mechanism has been proposed for CeO_2[30] and Y_2O_3[31] in which the grain boundary mobility is suppressed by the presence of oxygen interstitials. A similar phenomenon has been observed for bulk-UO_2. Compared with pure UO_2, titania-doped UO_2[32] is not only found to have faster grain growth rate, but also higher activation energy.

4 | CONCLUSIONS

Dense nano-sized UO_{2+x} with controlled stoichiometries and grain sizes were fabricated by SPS, and their microstructure evolution upon isothermal annealing and grain growth kinetics were studied with focus on grain growth, pore coarsening, and their interaction. Both hyper-stoichiometric $UO_{2.11}$ and more stoichiometric $UO_{2.03}$ experiences thermally

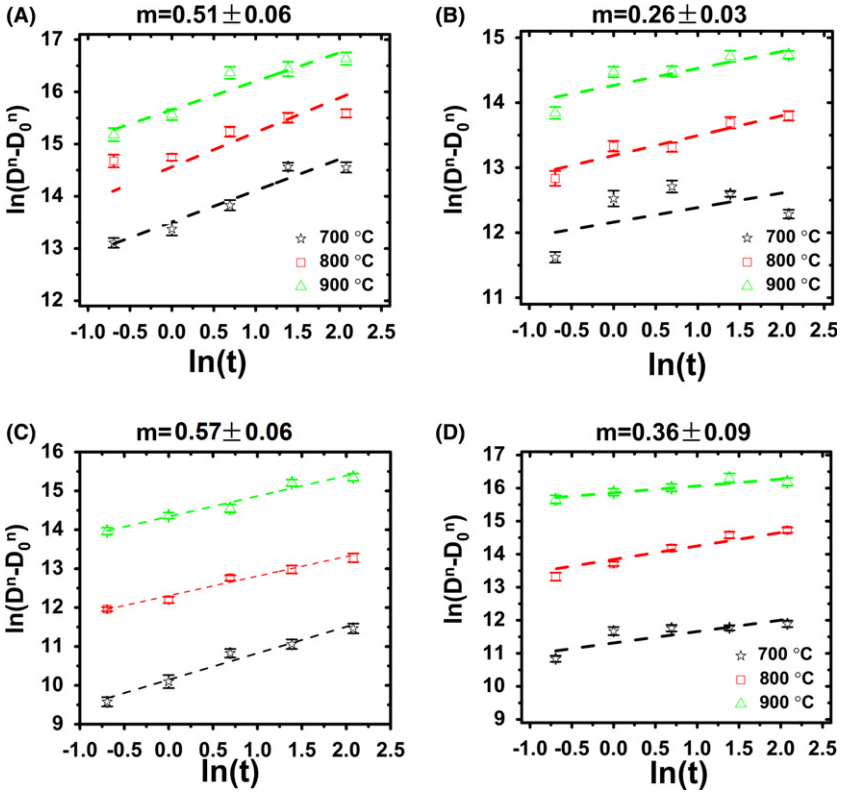

FIGURE 6 Grain coarsening and time components for (A) the $UO_{2.03}$-103 nm, (B) $UO_{2.03}$-144 nm, (C) $UO_{2.11}$-66 nm, and (D) $UO_{2.11}$-165 nm pellets [Color figure can be viewed at wileyonlinelibrary.com]

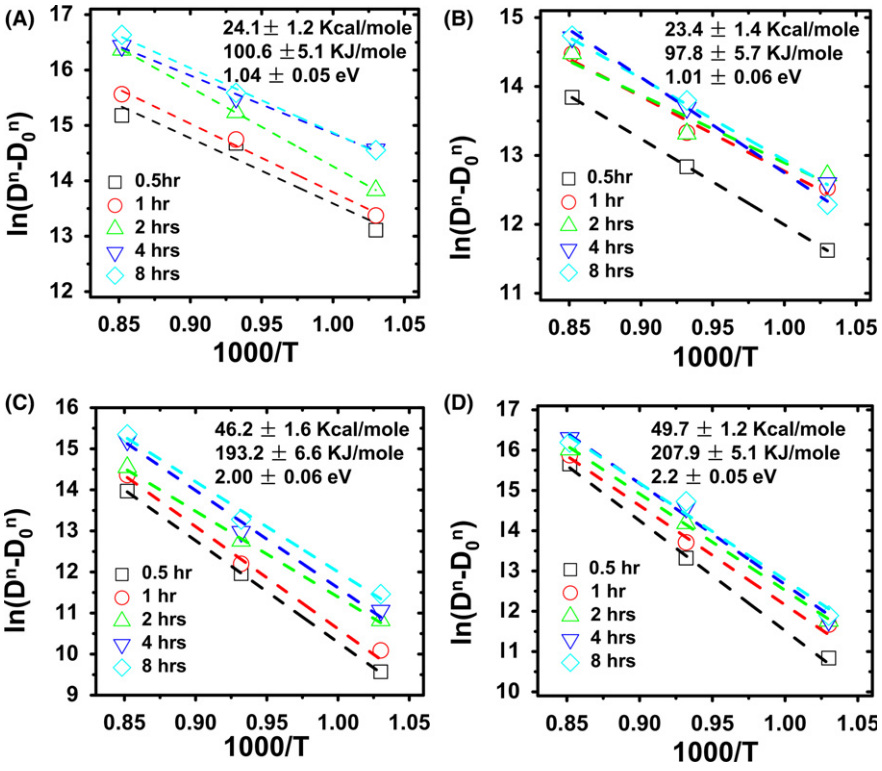

FIGURE 7 Grain growth kinetics for (A) $UO_{2.03}$-103 nm, (B) $UO_{2.03}$-144 nm, (C) $UO_{2.11}$-66 nm, and (D) $UO_{2.11}$-165 nm pellets with determined grain growth activation energies presented in three different units [Color figure can be viewed at wileyonlinelibrary.com]

induced grain coarsening and pore coalescence. Larger grain sizes were observed in nano-sized $UO_{2.11}$ as compared $UO_{2.03}$ with different grain growth kinetics. Derived grain growth exponents indicate that nano-sized UO_{2+x} generally follows the classical grain coarsening mechanism upon isothermal annealing, and the activation energy of grain coarsening is significantly lower than that of the bulk counterpart. Grain boundary diffusion may dominate the grain growth kinetics of the nano-sized UO_{2+x}, depending on the grain size and stoichiometry of the fuel matrix.

ACKNOWLEDGMENT

The work on grain size refinement by high-energy ball-milling and powder stoichiometry control was financially supported by the NSF career award DMR 1151028. The work on spark plasma sintering of nano-sized dense UO_{2+x} pellets, isothermal annealing, and grain coarsening was supported by the US DOE Nuclear Energy University Program (NEUP) under the award of DE-NE0008440 and the US DOE Nuclear Energy Advanced Modeling and Simulation (NEAMS) program. Argonne's work was supported by the U.S. Department of Energy under Contract No. DE-AC-02-06CH11357 between UChicago Argonne, LLC and the Department of Energy.

REFERENCE

1. Rondinella VV, Wiss T. The high burn-up structure in nuclear fuel. *Mater Today*. 2010;13:24–32.
2. Spino J, SantaCruz H, JovaniAbril R, Birtcher R, Ferrero C. Bulk-nanocrystalline oxide nuclear fuels – an innovative material option for increasing fission gas retention, plasticity and radiation-tolerance. *J Nucl Mater*. 2012;422:27–44.
3. Degueldre C, Bertsch J, Kuri G, Martin M. Nuclear fuel in generation II and III reactors: research issues related to high burn-up. *Energy Environ Sci*. 2011;4:1651–1661.
4. Ainscough JB, Oldfield BW, Ware JO. Isothermal grain growth kinetics in sintered UO2 pellets. *J Nucl Mater*. 1973;49:117–128.
5. Hastings IJ. Grain growth in UO2: in-reactor and laboratory testing. *J Nucl Mater*. 1979;82:435–438.
6. Tonks MR, Gaston D, Millett PC, Andrs D, Talbot P. An object-oriented finite element framework for multiphysics phase field simulations. *Comput Mater Sci*. 2012;51:20–29.
7. Sokol M, Kalabukhov S, Dariel M, Frage N. High-pressure spark plasma sintering (SPS) of transparent polycrystalline magnesium aluminate spinel (PMAS). *J Eur Ceram Soc*. 2014;34:4305–4310.
8. Teske K, Ullmann H, Rettig D. Investigation of the oxygen activity of oxide fuels and fuel-fission product systems by solid electrolyte techniques. Part I: qualification and limitations of the method. *J Nucl Mater*. 1983;116:260–266.
9. Sokol M, Kalabukhov S, Dariel MP, Frage N. High-pressure spark plasma sintering (SPS) of transparent polycrystalline magnesium aluminate spinel (PMAS). *J Eur Ceram Soc*. 2014;34:4305–4310.
10. Schneider CA, Rasband WS, Eliceiri KW. NIH Image to ImageJ: 25 years of image analysis. *Nat Meth*. 2012;9:671–675.
11. Desgranges L, Baldinozzi G, Rousseau G, Nièpce J-C, Calvarin G. Neutron diffraction study of the in situ oxidation of UO2. *Inorg Chem*. 2009;48:7585–7592.
12. Wang J, Ewing RC, Becker U. Average structure and local configuration of excess oxygen in UO_{2+x}. *Sci Rep*. 2014;4:4216.
13. Naito K, Tsuji T, Matsui T. Defect structure and the related properties of UO_2 and doped UO_2. In: Nowotny J, Weppner W, eds. *Non-Stoichiometric Compounds*, vol. 276. NATO ASI Series. AH Dordrecht, the Netherlands: Springer; 1989:27–44.
14. Dehaudt P, Bourgeois L, Chevrel H. Activation energy of UO_2 and UO_{2+x} sintering. *J Nucl Mater*. 2001;299:250–259.
15. Sari C. Grain growth kinetics in uranium-plutonium mixed oxides. *J Nucl Mater*. 1986;137:100–106.
16. Amato I, Colombo R, Protti A. Influence of stoichiometry on the rate of grain growth of UO_2. *J Am Ceram Soc*. 1963;46:407–07.
17. Marin JF, Contamin P. Uranium and oxygen self-diffusion in UO_2. *J Nucl Mater*. 1969;30:16–25.
18. Van Uffelen P, Botazzoli P, Luzzi L, et al. An experimental study of grain growth in mixed oxide samples with various microstructures and plutonium concentrations. *J Nucl Mater*. 2013;434:287–290.
19. He H, Shoesmith D. Raman spectroscopic studies of defect structures and phase transition in hyper-stoichiometric UO_{2+x}. *Phys Chem Chem Phys*. 2010;12:8108–8117.
20. Kapadia C, Leipold M. The mechanism of grain growth in ceramics. *N73-32435*, 1972;1–51.
21. Ahmed K, Pakarinen J, Allen T, El-Azab A. Phase field simulation of grain growth in porous uranium dioxide. *J Nucl Mater*. 2014;446:90–99.
22. Matzke H. On uranium self-diffusion in UO_2 and UO_{2+x}. *J Nucl Mater*. 1969;30:26–35.
23. Tonks MR, Zhang Y, Bai X, NEAMS FPL M2 milestone report: development of a UO_2 grain size model using multicale modeling and simulation. Idaho National Laboratory (INL) 2014.
24. Hawkins RJ, Alcock CB. A study of cation diffusion in UO_{2+x} and ThO_2 using α-ray spectrometry. *J Nucl Mater*. 1968;26:112–122.
25. Yajima S, Furuya H, Hirai T. Lattice and grain-boundary diffusion of uranium in UO_2. *J Nucl Mater*. 1966;20:162–170.
26. Auskern AB, Belle J. Oxygen ion self-diffusion in uranium dioxide. *J Nucl Mater*. 1961;3:267–276.
27. Sabioni ACS, Ferraz WB, Millot F. Effect of grain-boundaries on uranium and oxygen diffusion in polycrystalline UO_2. *J Nucl Mater*. 2000;278:364–369.
28. Vincent-Aublant E, Delaye J, Van Brutzel L. Self-diffusion near symmetrical tilt grain boundaries in UO_2 matrix: a molecular dynamics simulation study. *J Nucl Mater*. 2009;392:114–120.
29. Florence T, A review and comparison of method for the determination of the oxygen/uranium ratios in uranium oxides. In *Proceedings of a Symposium on Analytical Methods in the Nuclear Fuel Cycles*. Vienna, Austria: IAEA; 1971:45–56.
30. Chen P-L, Chen IW. Grain growth in CeO_2: dopant effects, defect mechanism, and solute drag. *J Am Ceram Soc*. 1996;79:1793–1800.
31. Chen P-L, Chen IW. Grain boundary mobility in Y_2O_3: defect mechanism and dopant effects. *J Am Ceram Soc*. 1996;79:1801–1809.
32. Amato I, Colombo RL, Balzari AP. Grain growth in pure and titania-doped uranium dioxide. *J Nucl Mater*. 1966;18:252–260.

How to cite this article: Yao T, Mo K, Yun D, Nanda S, Yacout AM, Lian J. Grain growth and pore coarsening in dense nano-crystalline UO_{2+x} fuel pellets. *J Am Ceram Soc*. 2017;100:2651–2658.